Journal of Molecular Structure 1173 (2018) 512–520

Contents lists available at ScienceDirect

Journal of Molecular Structure

journal homepage: http://www.elsevier.com/locate/molstruc

Bromo-substituted cibalackrot backbone, a versatile donor or acceptor main core for organic optoelectronic devices

Haluk Dinçalp [a, *], Gözde Murat Saltan [a], Ceylan Zafer [b], Deniz Aykut Kıymaz [b]

[a] Department of Chemistry, Faculty of Arts and Science, Manisa Celal Bayar University, Yunus Emre, 45140 Manisa, Turkey
[b] Solar Energy Institute, Ege University, Bornova, 35100 Izmir, Turkey

ARTICLE INFO

Article history:
Received 10 September 2017
Received in revised form
10 June 2018
Accepted 3 July 2018
Available online 11 July 2018

Keywords:
Cibalackrot
Organic photovoltaic
Electron mobility
Charge transfer
Decay time

ABSTRACT

Cibalackrot (**Ci-I**), one of the latest highly conjugated compound possessing *bis*-lactam structure, was investigated with respect to their brominated derivatives in order to determine their suitable substitution points for the syntheses of new class of small molecules for optoelectronic devices. 7,14-*Bis*(4-bromophenyl) (**Ci-II**) and 3,10-dibromo (**Ci-III**) derivatives of cibalackrot possess moderately narrow band gaps of 2.15 and 2.09 eV, respectively. Notably, **Ci-III** dye exhibits more red-shifted ultraviolet −visible (UV−vis) absorption and fluorescence emission spectra as compared to that of **Ci-II** dye because **Ci-III** shows more prominent intramolecular charge transfer (ICT) complex than that of **Ci-II** dye. Electron mobilities of the order of 7.0×10^{-4} cm^2/V and 3.1×10^{-4} cm^2/V were measured using **Ci-II** and **Ci-III** as active layer, respectively. Charge transfer properties of the molecules were investigated in bulk heterojunction device configuration wherein **Ci-III** showed p-type behavior against n-type PCBM in photovoltaic device. Photovoltaic performance of **Ci-III** dye which was used as donor component is 20 times higher than that of the device in which this dye was used as acceptor.

1. Introduction

Nowadays, there are increasing efforts on structural variations of conjugated polymers and small molecules for optoelectronic devices in order to obtain the most suitable structural design for managing high performance devices. Such kind of variations tailored by electron donor (D) and electron-acceptor (A) groups of the main core have great impact on optoelectronic parameters such as optical bandgaps, fluorescence characteristics, absorption profiles, and ionization potentials [1]. Organic photovoltaics (OPVs) have gained a considerable attention in the area of solar light-energy conversion systems owing to their low cost, flexibility and remarkable lightweight [2]. A considerable tendency of the molecular design for OPVs are externalized on attachment of different D or A subunits to the suitable position of the electroactive backbone. These provide a wide range of molecular arrangements of functional molecules for OPVs.

Among the several small organic molecules with electroactive core, cibalackrot dye [3,4], a bay-annulated indigo derivative, has received considerable attention for its excellent ambipolar charge transport property [5,6], high conjugated structure, excellent electron acceptor property [7], high fluorescence quantum yield [8], low-lying LUMO energy level, and narrow optical band gap [9]. Cibalackrot dye gives long-wavelength absorption profile with its maximum absorptions around 540–560 nm [8] due to the enhanced π-electron resonance localized between the indole and lactam segments of the structure. Typically, it is noted that strongly-bound localized excitons in the highly-disordered organic semiconductors are the result of low dielectric constant. Higher dielectric constants can be observed in molecules with the higher degree of order such as cibalackrot dyes ($\varepsilon = 4.8$) as compared to indigo dyes ($\varepsilon = 4.3$) [7]. Proton transfer pathway through intramolecular hydrogen bond is blocked because of highly-annulated structure of cibalackrot as compared to that of indigo/tyrian purple type dyes, which exhibit an efficient excited state deactivation pathway due to the proton-exchange mechanism [7,8].

Noting that annulation pathway through cibalackrot ring opens up new category of design for acceptor type molecules. In cibalackrot platform, oxindole units of indigo are fixed into a coplanar geometry where carbonyl groups and nitrogen atoms are annulated through acetyl chloride group to form *bis*-lactam structure of cibalackrot [6,10].

Despite these advantages of cibalackrot dyes over other organic

* Corresponding author.
E-mail address: haluk.dincalp@cbu.edu.tr (H. Dinçalp).

https://doi.org/10.1016/j.molstruc.2018.07.009
0022-2860/

molecular acceptors, there are limited number of their applications in OPV devices. To the best of our knowledge, only few attempts have been made to investigate OPV devices using cibalackrot dye as the photo-active layer. Bronstein et al. reported charge transport and photodiode properties of a cibalackrot polymer in organic electronic devices. This polymer exhibits high ambipolar transport in OFET device of 0.23 cm^2/V, and also OPV device efficiencies up to 2.35% [11]. Liu et al. explored the electrochromic efficiency of a cibalakrot polymer giving high optical contrast in the visible and near-infrared region, good coloration efficiency and long term stability [12].

In this work, cibalackrot core was brominated to its phenyl or indole rings (Scheme 1) in order to investigate the relationship between substitution points of the structure and photovoltaic performance. Their absorption-emission profiles and fluorescence decay kinetics were investigated in different solvents of polarities. Their electrochemical properties were evaluated in electron mobility measurements and photovoltaic performances.

2. Experimental

2.1. Materials and reagents

The main reagents used for the synthesis of cibalackrot dyes, 4-Bromo-2-nitrobenzaldehyde and phenylacetyl chloride were purchased from Sigma Aldrich and Merck Company, respectively. *Tetrakis*(triphenylphosphine)palladium(0) ($Pd(PPh_3)_4$) catalyst was purchased from TCI company. All other chemicals and solvents were purchased from Merck, and used without further purification. Photovoltaic materials [6,6]-Phenyl C_{61}-butyric acid methyl ester (PCBM) and poly(3-hexylthiophene-2,5-diyl) (P3HT) were purchased from Sigma Aldrich.

2.2. Analytical instruments

^1H and ^{13}C NMR spectra were obtained using a Bruker 400 MHz spectrometer. Chemical shifts were reported as ppm relative to the TMS standard (0 ppm). FT-IR spectra were monitored on a Perkin Elmer-Spectrum BX spectrophotometer with samples prepared as KBr pellets. The optical properties of the dyes were investigated by both UV–Vis spectroscopy using a Perkin Elmer Lambda 950 spectrophotometer and fluorescence emission spectroscopy using a FLS 920 Edinburg instrument in different solvent of polarities in 1 cm optical path length cuvettes. Single photon counting results and fluorescence decays were analyzed globally using the Edinburgh Instruments F900 exponential tail fit method [13] at the excitation wavelength of 472.4 nm. The quality of the fits has been judged by the fitting parameters such as $\chi^2 \leq 1.2$ [14]. All spectroscopic measurements in solution were done at optical density around 0.1.

2.3. Electrochemical measurements and DFT calculations

The electrochemical properties of the dyes were performed in an acetonitrile solution with 0.1 M tetrabutylammoniumhexafluorophosphate [TBA][PF_6] as the supporting electrolyte, glassy carbon as the working electrode, a Pt wire as the counter electrode, and a Ag/Ag^+ as the reference electrode using a CH instrument (660B-Electrochemical Workstation) at a scan rate of 100 mV s^{-1}. Potentials were referenced to the ferrocenium/ferrocene redox couple by using ferrocene as an internal standard and its oxidation potential was detected at +0.63 V. Onset values of E_{red}, E_{ox}, and other parameters were calculated according to the equation [15]:

$$E_{HOMO} = -e(E_{ox}^{onset} + 4.8); E_{LUMO} = -e(E_{red}^{onset} + 4.8)$$

$$E_g^{opt} = {}^{1240}\!/\!_{\lambda_{abs}^{onset}};\ E_{HOMO} = E_{LUMO} - E_g^{opt}$$

The electronic structures of **Ci-II** and **Ci-III** molecules were investigated using DFT and TD-SCF [16] with B3LYP/6-31G(d) basis [17], as implemented in the Gaussian 09 package. The UV–vis absorption spectra of **Ci-II** and **Ci-III** dyes were also calculated by TD-SCF. Oscillator strength (f) calculated by time dependent density functional theory were presented as 0.7063, and 0.5475 for **Ci-II** and **Ci-III**, respectively.

2.4. Fabrication and characterization of OPV devices

Indium tin oxide (ITO) deposited glass substrates from Delta Tech. Corp. (2.5 × 2.5 cm in size) with R_{sheet}: 10 Ω/sq conductivity were cleaned using a deionized water, acetone, and isopropanol for 10 min each by sonication, and dried under a stream of nitrogen.

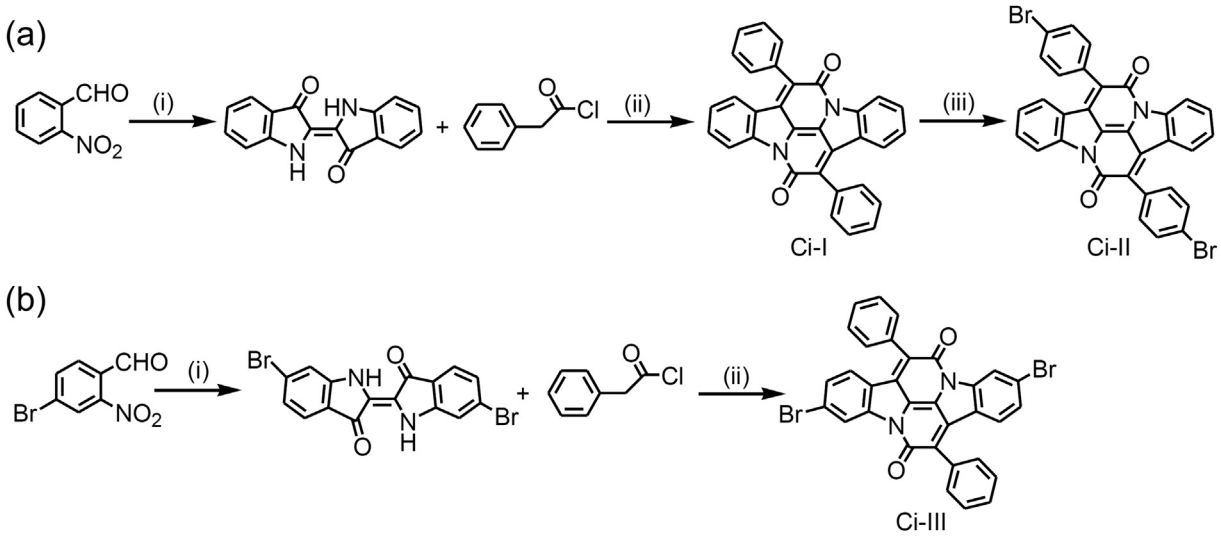

Scheme 1. Synthesis of (a) **Ci-II** and (b) **Ci-III** dyes. **(i)** Acetone:water (1:1), NaOH, ice bath, then room temperature [4]; **(ii)** xylene, 140 °C, 48 h, reflux [8]; **(iii)** N-bromosuccinimide, $CHCl_3$, room temperature [6].

Then, the ITO substrates were treated with UV oxygen plasma with a 100 W power for 5 min under 10^{-2} mbar pressure. The PEDOT:PSS solution was diluted with pure water to a ratio of 1:1 (by volume) and filtrated through the 0.45 μm PTFE syringe filter prior to use and spin-coated at a speed of 4000 rpm for 30 s, resulting in a layer with a thickness 40 nm. The PEDOT:PSS-coated ITO substrates were dried in a vacuum oven at 120 °C for 15 min. Solutions of photo-active components in 1,2-dichlorobenzene:chloroform (7:3 *v*/*v*) were mixed at concentrations of 2 or 4 wt% in different mass ratios and stirred overnight. The pre-formed solutions of P3HT, PCBM, and **Ci-(I-III)** dyes were spin-coated (1500 rpm for 1 min), and dried at 120 °C for 15 min in a N_2 filled atmosphere, giving in a layer with a thickness 80 nm. The LiF/Al (0.6 nm/70 nm) metal electrode was thermally deposited. All of the device fabrication characterization processes were carried out under N_2 atmosphere in MBRAUN 200B glove box.

The current density versus voltage (J–V) characteristics were recorded on a Keithley model 2400 source meter unit and LabVIEW® data acquisition software in the dark and under simulated AM1.5G illumination with intensity of 100 mW/cm^2 using ATLAS Solar Test (75 W) solar simulator integrated to glove box.

For electron mobility measurements, electron-only devices were fabricated and the mobilities were determined by fitting the dark current using an equation given below:

$$J_{SCLC} = \frac{9}{8}\varepsilon_0\varepsilon_r\mu_e\frac{V^2}{L^3}$$

where ε_o is the permittivity of free space, ε_r is the dielectric constant of the Ret film, μ_e is the electron mobility, V is the applied voltage and L is the thickness of the photo-active layer [18,19].

2.5. Synthesis procedures

2.5.1. General procedures for the synthesis of Indigoid dyes:

Nitrobenzaldehyde derivatives (1 mmol) were dissolved in 20 mL of acetone:water (1:1 *v*/*v*). After cooling to −5 °C, 5 mL aqueous solution of 1 M NaOH was added dropwise to adjust the pH to 10. The mixture was stirred overnight at room temperature. The resulting precipitate was collected by suction filtration, and then precipitates were washed with acetone and distilled water until washings ran colorless.

2.5.1.1. Synthesis of indigo dye. 2-Nitrobenzaldehyde was used in the reaction. Indigo was obtained as a blue solid, yielding 48%. FT-IR (KBr pellet, cm^{-1}): 3264, 1710 (ketone $\nu_{C=O}$), 1625, 1613, 1585 (aromatic $\nu_{C=C}$), 1489, 1461, 1392, 1316, 1298, 1197, 1173, 1126, 1095, 1068, 878, 712 cm^{-1}.

2.5.1.2. Synthesis of tyrian purple dye. 4-Bromo-2-nitrobenzaldehyde was used in the reaction. Tyrian purple was obtained as a purplish powder, yielding 42%. FT-IR (KBr pellet, cm^{-1}): 3640, 3386 (amine ν_{N-H}), 2955 (aromatic ν_{C-H}), 1706 (ketone $\nu_{C=O}$), 1634, 1614, 1578, 1532, 1439, 1387, 1313, 1231, 1158, 1047, 898, 767 cm^{-1}.

2.5.2. General procedures for synthesis of cibalackrot dyes

To a refluxing xylene (30 mL) solution of indigoid dye (1 mol equiv.) was added phenylacetyl chloride (12 mol equiv.) dropwise under an argon flow. The mixture was refluxed for 48 h, and then cooled down to room temperature. The precipitate was collected by suction filtration, and washed with ethanol and ether, respectively, to give cibalackrot derivative as a red solid.

*2.5.2.1. Synthesis of cibalackrot dye (**Ci-I**).* Yield 45%, FT-IR (KBr pellets, cm^{-1}): 3431, 2921, 1632, 1480, 1415, 1313, 1267, 1080, 984, 763 cm^{-1}.^{1}H NMR (400 MHz, $CDCl_3$ δ 7.27 ppm) δ 8.52 (d, J = 7.8 Hz, 2H), 7.76–7.73 (m, 4H), 7.61–7.55 (m, 8H), 7.22 (d, J = 7.8 Hz, 4H) ppm. ^{13}C NMR [(100 MHz, $CDCl_3$ δ 77.45 (3 peaks)] δ 156.8, 149.7, 145.6, 135.9, 134.8, 134.3, 132.9, 130.8, 129.9, 129.3, 126.8, 126.3, 126.2, 118.3 ppm.

*2.5.2.2. Synthesis of 3,10-dibromo-7,14-diphenyldiindolo[3,2,1-de:3′,2′,1′-ij]-1,5- naphtydridine-6,13-dione (**Ci-III**).* Yield 52%, FT-IR (KBr pellets, cm^{-1}): 3432, 1735 (amide $\nu_{C=O}$), 1628, 1597, 1419, 1275, 1075, 699 cm^{-1}.^{1}H NMR (400 MHz, DMSO-d_6 δ 2.49 ppm): δ = 7.31 (d, J = 1.2 Hz, 2H), 7.30–7.28 (m, 6H), 7.24 (d, J = 2.5 Hz, 4H), 7.22 (d, J = 2.5 Hz, 4H) ppm. ^{13}C NMR [100 MHz, $CDCl_3$ δ 76.9 (3 peaks)]: δ = 176.6, 158.8, 153.4, 141.2, 133.1, 130.4, 129.9, 129.6, 129.5, 129.3, 128.6, 128.4, 127.3, 127.0 ppm.

*2.5.2.3. Synthesis of 7,14-bis(4-bromophenyl)diindole-[3,2,1-de:3′,2′,1′-ij]-1,5-naphtydridine-6,13-dione (**Ci-II**).* To solution of **Ci-I** (112 mg, 0.24 mmol) in chloroform (14 mL) was added N-bromosuccinimide (NBS) (93 mg, 0.52 mmol) slowly. The mixture was stirred at room temperature for 16 h. Then, the organic phase was washed with distilled water (3 × 50 mL). Solvent was removed by rotary evaporation under reduced pressure to give **Ci-II** as a red solid, yielding 80%. FT-IR (KBr pellets, cm^{-1}): 3441, 2957, 1770 and 1701 (amide $\nu_{C=O}$), 1631, 1488, 1415, 1321, 1262, 1167, 1080, 1020, 802, 762 cm^{-1}.^{1}H NMR (400 MHz, $CDCl_3$ δ 7.26 ppm) δ 7.72 (d, J = 7.1 Hz, 2H), 7.55 (d, J = 9.1 Hz, 8H), 7.33 (s, 6H) ppm.

3. Results and discussion

3.1. Steady state measurements

Optical absorption profiles of synthesized cibalackrot dyes in solution and on thin-film states are illustrated in Fig. 1, and corresponding optical data are summarized in Table 1. The visible absorption spectra of these dyes in benzonitrile were composed of two main absorption maxima at 548 nm and 512 nm for **Ci-II** dye, while that was 557 nm and 518 nm for **Ci-III** dye, as shown in Fig. 1a. Concentration experiments have been made for both **Ci-II** and **Ci-III** dyes in chloroform solution in order to understand whether the aggregates formed or not. Fig. S1a and b shows the concentration experiments for **Ci-II** and **Ci-III** dyes, respectively. According to the spectra, shapes and the positions of the peaks in the visible region remained unchanged. This observation indicates that aggregation does not observed for both dyes. Existence of the long-wavelength absorption bands of the dyes could not be explained by the aggregation behavior. The shoulder bands in the higher energy region can be attributed to $\pi-\pi^*$ transition. The strongest absorption bands in the lower energy region can be attributed to intramolecular charge transfer (ICT) complex, previously described for cibalackrot type dyes in the literature [6,9,12]. From the observational evidence in this work, ICT formed in **Ci-III** dye is more prominent than that of **Ci-II** dye so that the maximum and the shoulder of the absorption bands of **Ci-III** are more shifted to red region in the studied solvents as compared to that of **Ci-II**. This red-shifted absorption is also attributed to the auxochrome Br atoms which can give their non-bonding electrons to the aromatic core through conjugated structure.

Fig. 1b gives a comparison visible absorption spectra of **Ci-III** dye in different solvent of polarities. Notably, there is a marked red-shift of 29 nm in the long-wavelength absorption maximum of **Ci-III** dye as compared to that of **Ci-II** dye in ethyl acetate solution. Also, when compared to other studied solvents, absorption profile of **Ci-III** dye shows more bathochromic shifts in ethyl acetate. These results are more consistent with much higher polarizability of the excited dye structure with respect to its ground state in ethyl acetate solution,

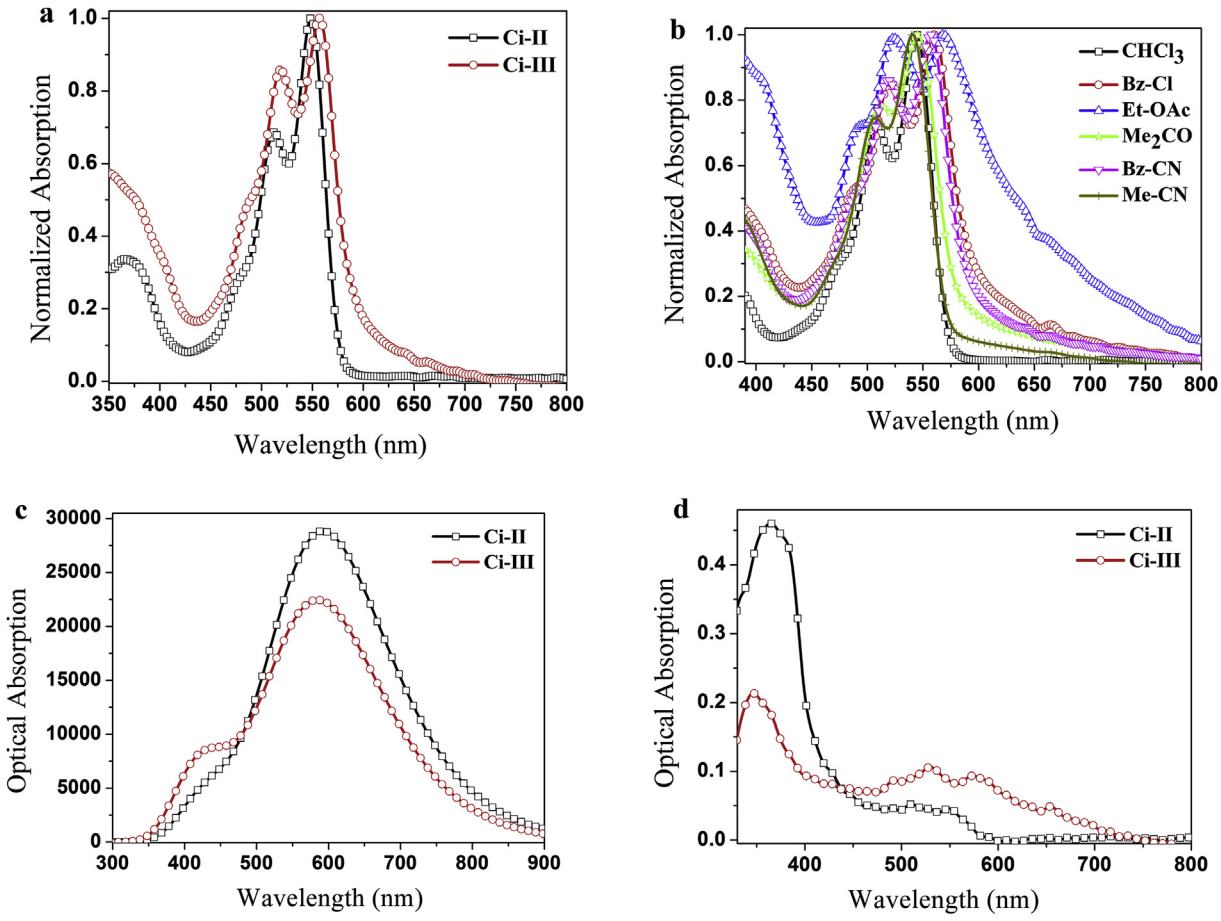

Fig. 1. **(a)** Comparison of the normalized UV–vis absorption spectra of **Ci-II** and **Ci-III** dyes in BzCN solution. **(b)** Normalized UV–vis absorption spectra of **Ci-III** dye in different solvents. **(c)** UV–vis absorption spectra of **Ci-II** and **Ci-III** dyes calculated by TD-SCF. **(d)** Optical absorption of **Ci-II** and **Ci-III** films on ITO-coated substrate.

Table 1
Long-wavelength absorption (λ (nm)) and emission wavelengths (λ_{em} (nm)) of **Ci-II** and **Ci-III** dyes in different solvents ($\lambda_{exc} = 485$ nm).

Dyes/Solvents	**Ci-II**				**Ci-III**			
	λ_1	λ_2	λ_{em1}	λ_{em2}	λ_1	λ_2	λ_{em1}	λ_{em2}
$CHCl_3$	538	503	600	560	545	507	609	568
BzCl	552	514	618	575	561	520	625	580
EtAc	540	506	606	562	569	523	615	570
Me_2CO	540	502	602	560	546	510	610	567
BzCN	548	512	615	572	557	518	619	578
MeCN	535	500	600	557	541	505	605	562

which then lowers the LUMO energy level of **Ci-III** dye. Both dyes give the lowest absorption wavelength numbers in more polar MeCN solution due to the existence of much lower polarizabilities of the dyes in the excited state. TDDFT calculations of the dyes exhibit one broad absorption band which corresponds to the combination of $\pi-\pi^*$ and ICT absorption for each dye, as shown in Fig. 1c. TDDFT calculations on UV–vis spectra did not show the charge transfer shoulder, and finally computed spectra showed a little red shift as compared to the experimental measurements. The absorption bands of **Ci-II** and **Ci-III** dyes in the film are significantly broadened, and are slightly red shift with a huge shoulder below 400 nm, as illustrated in Fig. 1d. These observations indicate the strong molecular stacking of the molecules in solid state.

Fig. 2a gives a comparison of the normalized fluorescence emission spectra of **Ci-II** and **Ci-III** dyes in benzonitrile solution at the excitation wavelength of 485 nm. **Ci-II** dye exhibits emission maximum at 572 nm with a shoulder at 615 nm in benzonitrile. **Ci-III** dye gives a red shift of 4–6 nm with respect to **Ci-II** dye. The most red-shifted emission maximum for **Ci-II** dye was observed at 618 nm in chlorobenzene solution, as shown in Fig. 2b. In acetonitrile solution, both dyes gave more blue shifts in their emission maxima, monitoring at wavelengths of λ_{em1}:600, λ_{em2}:557 nm for **Ci-II** dye and λ_{em1}:605, λ_{em2}:562 nm for **Ci-III** dye. Fig. 2c gives the excitation spectra of **Ci-II** and **Ci-III** dyes in chlorobenzene solution at the collected emission wavelength of 575 nm. It is seen that excitation spectra of these dyes were almost similar to their absorption profiles. Noting that contaminants or any other reactive reagents are not existed in the excited state of the dyes.

Fluorescence decay time values and fluorescence quantum yields for both dyes were given in Table 2. Fig. 3 compares the time-resolved emission spectra for **Ci-II** dye in chloroform with benzonitrile solution in 450 ns time window. While the fluorescence decay times of **Ci-II** dye can be analyzed as mono-exponential decays around 4.29–6.78 ns, **Ci-III** dye gives bi-exponential decays with short decay times around 1.57–3.84 ns and long decay times around 6.36–10.37 ns in the studied solvents. A more detailed investigation of the time-decay profiles of cibalackrot dye was studied by Melo group in 2006. They reported the long-lived decay component of 6.10 ns for cibalackrot dye in dioxane [8]. In our measurements, the short decay times can be attributed to quench of direct emission of cibalackrot core for **Ci-III** dye. The long decay times between 6.36 and 10.37 ns with low amplitudes of

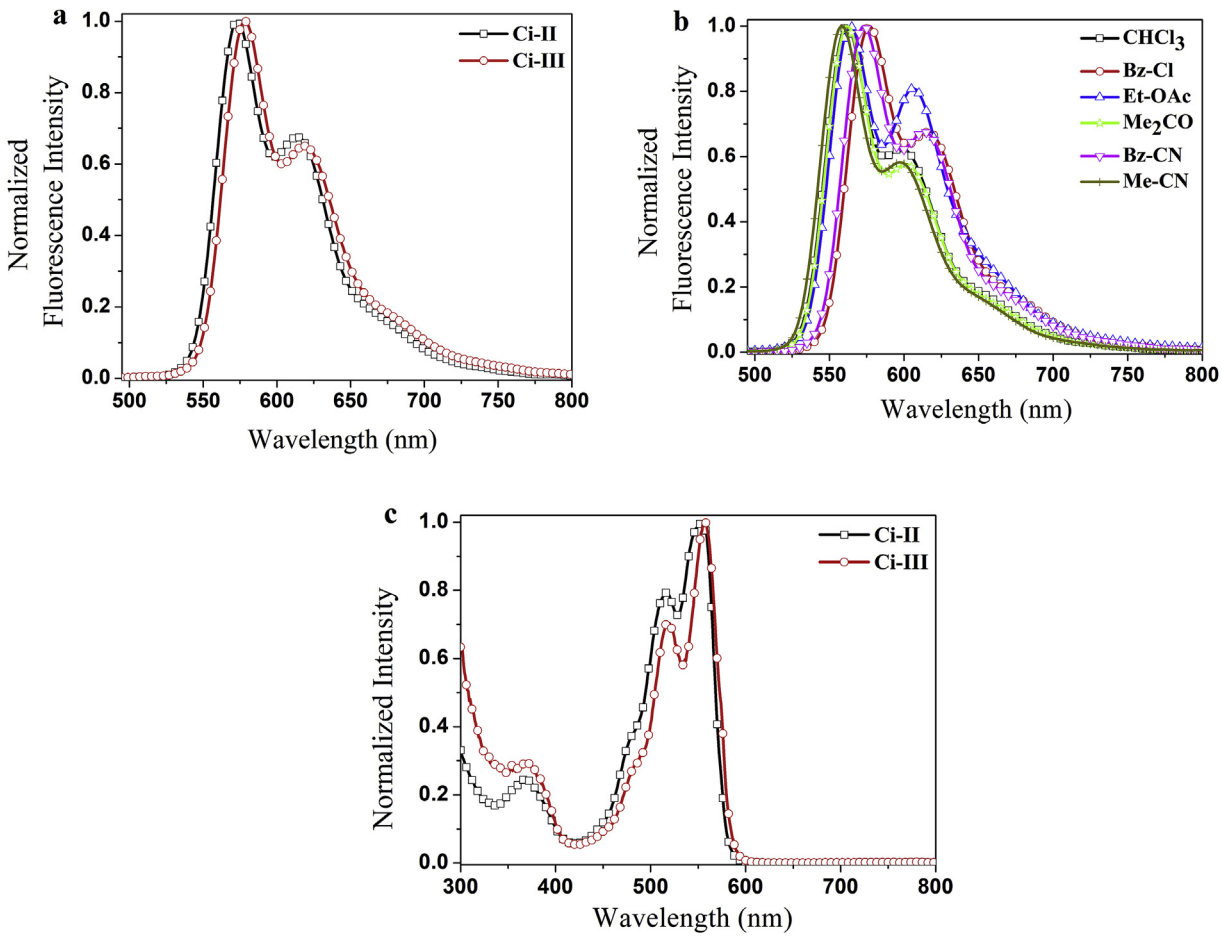

Fig. 2. **(a)** Comparison of the normalized fluorescence emission spectra of **Ci-II** and **Ci-III** dyes in BzCN solution. **(b)** Normalized fluorescence emission spectra of **Ci-II** dye in different solvents ($\lambda_{exc} = 485$ nm). **(c)** Excitation spectrum of **Ci-II** and **Ci-III** dyes in BzCl solution at the collected emission wavelength of 575 nm.

Table 2
Fluorescence quantum yields (ΦF) and fluorescence decay times (τf (ns)) with amplitudes of Ci-II and Ci-III dyes in different solvents (λexc = 485 nm, λdetection = 535 nm)[a].

Dyes/Solvents		χ^2	$\tau_{f(1)}$	α_1	$\tau_{f(2)}$	α_2	Φ_F
Ci-II	$CHCl_3$	0.90	4.29	100	–	–	0.64
	BzCl	0.92	6.78	100	–	–	0.66
	EtAc	0.99	6.03	100	–	–	0.40
	BzCN	1.11	6.12	100	–	–	0.71
Ci-III	$CHCl_3$	0.73	1.57	86.1	6.36	13.9	0.16
	BzCl	0.76	3.84	79.3	8.30	20.7	0.16
	EtAc	0.84	2.68	60.2	8.44	49.8	0.034
	BzCN	0.73	3.15	71.2	10.37	28.8	0.003

[a] Fluorescence quantum yields have been determined using perylene-3,4,9,10-tetracarboxylic-bis-N,N′-dodecyl diimide (N-DODEPER) ($\Phi_F = 1.0$ in chloroform) [20].

13.9%–49.8% may belong to the ICT complex of cibalackrot backbone in the excited state, which is generated by the possible charge transfer between the central donor nitrogens to the phenyl side on the whole surface of the dyes. We took additional measurements using acetone and acetonitrile solvents to span the polarity range of the used solvents (Table S1). There is no obvious change on emission spectra for ICT state as the solvent polarity increases. Similar results were obtained and both solvents gave mono-exponential decays for **Ci-II** dye and bi-exponential decays for **Ci-III** dye at collected data around 535 nm.

In order to clarify the ICT decays at long times, we have analyzed the decay spectra at different detected emission wavelengths of 400, 575, 615 and 750 nm (Table S2). Single photon timing measurements for both dyes gave bi-exponential decays only at longest emission wavelength of 750 nm. This observation is taken as the evidence for the formation of ICT state which is formed at the expenses of the locally excited (LE) state. Following excitation, ICT state becomes the lowest energy state for both dyes. Interestingly, the more red-shifted absorption and emission bands for **Ci-III** dye as compared to **Ci-II** dye may be attributed to electron acceptor strength of bromo-substituted phenyl side. It was noted that inductive effects of Br atoms slightly increase the formation of ICT complex between the donor group and fused phenyl side in **Ci-III** dye by enhancing the electron-withdrawing capacity of cibalackrot backbone.

As illustrated in Table 2, fluorescence quantum yields of **Ci-III** dye (Φ_F:0.003–0.16) are lower than that of **Ci-II** dye (Φ_F:0.40–0.71) in the studied solvents. Cibalackrot cannot give any intra- or

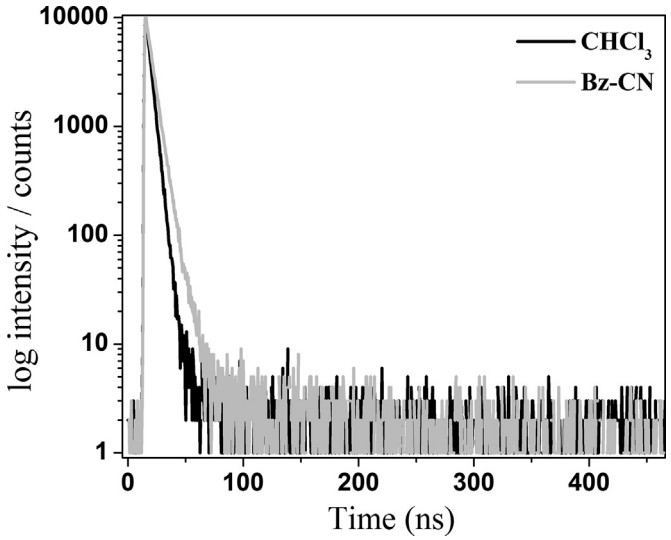

Fig. 3. Fluorescence decay graphs of **Ci-II** dye in $CHCl_3$ and BzCN solution ($\lambda_{detection} = 535$ nm).

intermolecular proton transfer reaction due to its rigid planar structure. This leads to high fluorescence quantum yields for cibalackrot core (Φ_F:0.76, in dioxane) [8]. However, **Ci-III** dye may not be completely rigid because of its possible conformational relaxation existed from the delocalization between bromine atoms and carbonyl groups in **Ci-III** dye whereas this is inhibited in **Ci-II** dye. This is responsible for much lower fluorescence quantum yields for **Ci-III** dye. A considerable ICT formation for **Ci-III** dye due to the inductive effect of Br atoms may also lead to the lower fluorescence quantum yields for **Ci-III** dye. Also, the lowest fluorescence quantum yields for **Ci-III** dye in ethyl acetate and benzonitrile solutions may be attributed to the self-quenching because of much possible aggregation behavior of the dye in these solutions.

3.2. Electrochemical properties

Fig. 4 shows the cyclic voltammograms of **Ci-II** and **Ci-III** dyes on glassy carbon working electrode in 0.1 M [TBA][PF_6]/Me-CN, and some important electrochemical data are summarized in Table 3.

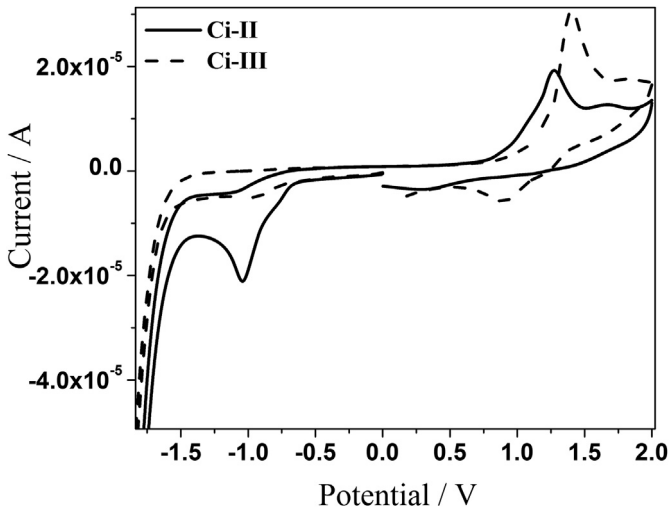

Fig. 4. Cyclic voltammograms of **Ci-II** and **Ci-III** dyes on glassy carbon working electrode in 0.1 M [TBA][PF6]/Me-CN (Scan rate: 100 mV s^{-1}).

Both **Ci-II** and **Ci-III** dyes show semi-reversible reduction and oxidation waves, which are corresponded to reduction of ketone groups and oxidation of tertiary amines, respectively. The oxidation and reduction potentials are 1.27 V and −1.04 V, respectively, vs. Ag/Ag^+ for **Ci-II** dye, 0.90 V (E^0_{ox2}:1.40 V), and −0.97 V, respectively, vs. Ag/Ag^+ for **Ci-III** dye, which correspond to HOMO and LUMO energy levels of −5.28 and −3.13 eV, respectively, for **Ci-II** dye and −5.29 and −3.20 eV, respectively, for **Ci-III** dye.

Changing the position of the Br-moiety from the phenyl to the indole group effects the oxidation and reduction behaviours of cibalackrot backbone. While electron withdrawing ability of Br facilitates the reduction of carboxyl group inductively in **Ci-III** dye, oxidation of the amine centre in this structure becomes more difficult due to reduced electron density. Therefore, oxidation of **Ci-III** dye was observed at higher potential (1.40 V), and its reduction (−0.97 V) was measured at lower potentials compared to **Ci-II** dye. In the case of **Ci-II**, inductive effect of the Br on the *p*-position of rotating phenyl moiety is not effective as much as being substituted directly to the conjugated indole centre.

The molecular orbital contours (Fig. 5) for the HOMO orbitals of both **Ci-II** and **Ci-III** dyes clearly show that the electron clouds lie mainly along with the axis of peripheral phenyl-lactam core, while for their LUMO orbitals, the electron density is concentrated equivalently on whole surface of the molecule. There is a substantial contribution to the LUMO from the fused phenyl rings of the structure. Substitution of this position will enable resulting the change of the LUMO energy level of the cibalackrot dye. As shown in Fig. 5, there is a little bit of energy gap between the LUMO level of **Ci-II** and **Ci-III** dyes (~0.07 eV).

3.3. Charge transfer performances

In order to analyze the electron only mobility characteristic of the dyes, we have used the devices for space-charge-limited current (SCLC) measurements like to solar cell with the structures of FTO/TiO_2(40 nm)/**Ci-(II-III)** (60 nm)/LiF(0.6 nm)/Al(70 nm). Fig. 6 gives the variation in the capacitance-frequency (C-F) characteristic of FTO/TiO_2/**Ci-II**/LiCl/Al device. Also, Fig. 7a and b represent the dark current density-effective voltage characteristics of SCLC mobilities in the device of FTO/TiO_2/**Ci-II**/LiCl/Al and FTO/TiO_2/**Ci-III**/LiCl/Al, respectively.

Ci-II and **Ci-III** dyes give the electron mobility values of 7.0×10^{-4} cm^2/V and 3.1×10^{-4} cm^2/V, respectively. Compared to reported FET values in the literature, we observed an order of magnitude lower transport rates [7]. Possible explanation of much lower mobilities can be a different transport mechanism in the bulk structure compared to surface transport. Degree of ordering and molecular packaging in crystalline structure is strongly effective on charge transport rates. Electron mobility values of **Ci-II** and **Ci-III** were found to be a nearly identical.

Performance capabilities of the synthesized dyes as acceptor or donor components in OPV devices have been evaluated on

Table 3
Electrochemical values and HOMO-LUMO energies of **Ci-II** and **Ci-III** dyes with respect to the vacuum level.

Dyes	E^0_{red1} (V)	E^0_{ox1} (V)	E^0_{ox2} (V)	LUMO (eV)	HOMO (eV)	$E_{0\text{-}0}$[a](eV) (abs)
Ci-I	−0.70	1.20	–	−3.47	−5.59	2.12
Ci-II	−1.04	1.27	–	−3.13	−5.28	2.15
Ci-III	−0.97	0.90	1.40	−3.20	−5.29	2.09

[a] The zeroth−zeroth transition E_{0-0} values were estimated from the intersection of the apsis and the straight line which is drawn from the red side of the UV−vis absorption band in chlorobenzene solution.

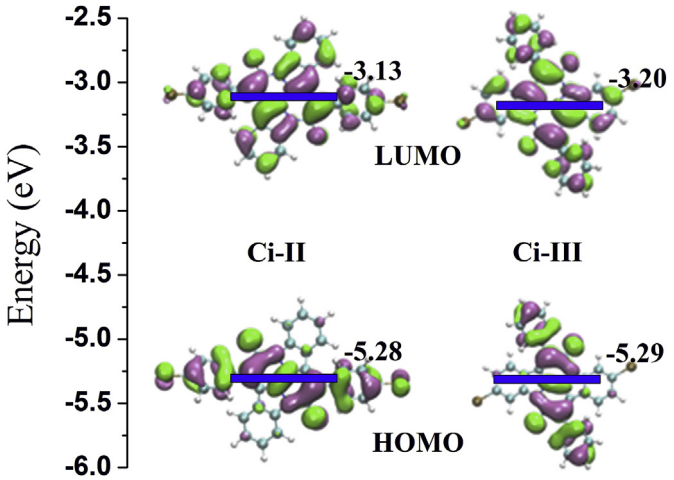

Fig. 5. Optimized ground-state geometries and frontier orbital energies of compounds **Ci-II** and **Ci-III** dyes obtained by TDDFT.

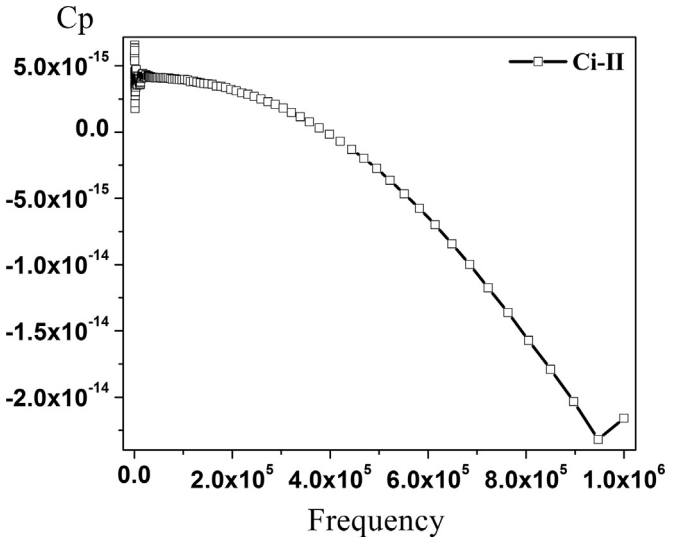

Fig. 6. The variation in the capacitance-frequency (C–F) characteristic of FTO/TiO_2/**Ci-II**/LiCl/Al device.

conventional devices using spin-coated films of P3HT as donor or fullerene as acceptor component, given below:

ITO/PEDOT:PSS/P3HT:**Ci-I**/LiF(0.6 nm)/Al(70 nm) (%2 w/w)
ITO/PEDOT:PSS/P3HT:**Ci-III**/LiF(0.6 nm)/Al(70 nm) (%4 w/w)
ITO/PEDOT:PSS/**Ci-III**:PCBM/LiF(0.6 nm)/Al(70 nm) (%4 w/w)

According to alignment of LUMO energy levels of **Ci-(I-III)** dyes with P3HT and PCBM, photovoltaic performances obtained from P3HT:**Ci-(I-III)** and **Ci-(I-III)**:PCBM donor-acceptor couples were predictable. There is an enough threshold for possible hole transfer between the HOMO levels of the dyes (−5.59 eV for **Ci-I**, −5.28 eV for **Ci-II**, and −5.29 eV for **Ci-III**) and P3HT donor (−5.1 eV) for the active layer of P3HT/dye in device configuration. On the other hand, LUMO energy level alignments of the synthesized dyes are favorable for an efficient electron transfer from their excited states to PCBM acceptor. Therefore, charge transfers between these donor-acceptor couples yield in higher efficiencies.

Fig. 8a, b and c give the J-V curves of P3HT:**Ci-I**, P3HT:**Ci-III** and **Ci-III**:PCBM blends as active layer in solar cell configurations. Table 4 summarizes the photovoltaic data obtained from the measurements. We couldn't obtain any photovoltaic signal with **Ci-II** dye in OPV device neither as p-type nor as n-type semiconductor. With the photovoltaic device based on P3HT:**Ci-I** (1:1) bulk heterojunction, efficiency of 0.003% with 220 mV open circuit voltage, 0.005 mA/cm^2 short circuit current and 0.5 fill factor was achieved, wherein the device based on P3HT:**Ci-III** (1:3 *w*/*w*) gave a V_{oc} of 40 mV, a J_{sc} of 0.060 mA/cm^2, a fill factor of 0.35 and a PCE of 0.001%. Remarkably, **Ci-III**:PCBM (1:4 *w*/*w*) based device presented an improved photovoltaic performance with a V_{oc} of 200 mV, a J_{sc} of 0.41 mA/cm^2, a fill factor of 0.28 and an increased PCE of 0.02%. These performances are below the previously reported OPV efficiency (2.35%) for a cibalackrot structure in the literature. Bronstein et al. used a conjugated thiophene polymer incorporated with cibalackrot backbone in conventional and inverted configuration of OPV device as donor component [11]. In our study, we examined the only pristine cibalackrot-bromine cores in OPV devices as acceptor or donor components without functionalizing them any polymeric fractions. These dyes without any polymeric groups can give a limited contribution to photocurrent due to their little energetic offset in IPCE spectra. Fig. 9 shows the IPCE graph for photovoltaic device using **Ci-III**:PCBM (1:4) blend as active layer. Blend exhibits a broad IPCE spectrum in accordance with the

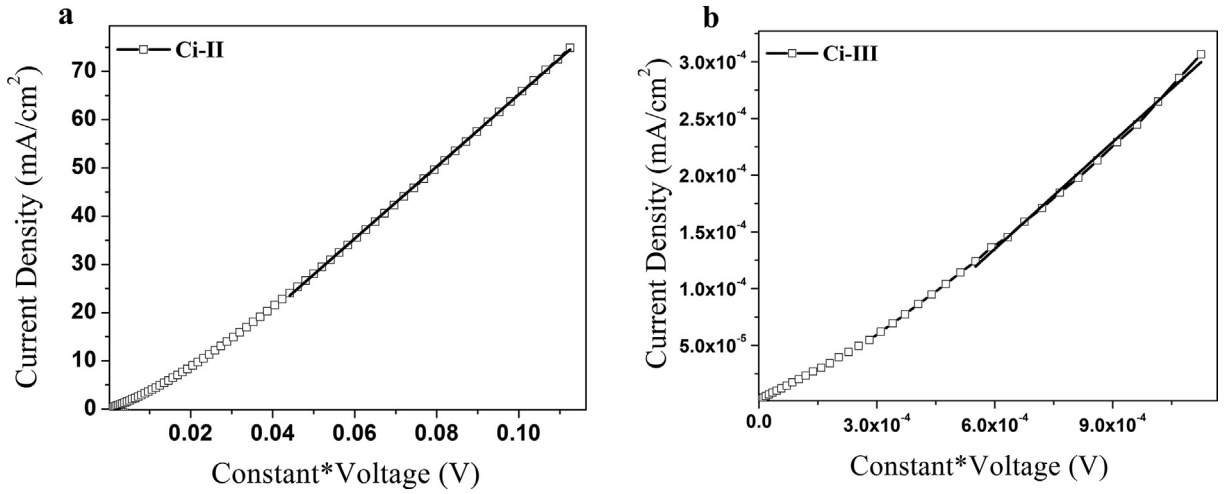

Fig. 7. Dark current density-effective voltage characteristics of SCLC mobilities in **(a)** FTO/TiO_2/**Ci-II**/LiCl/Al and **(b)** FTO/TiO_2/**Ci-III**/LiCl/Al devices.

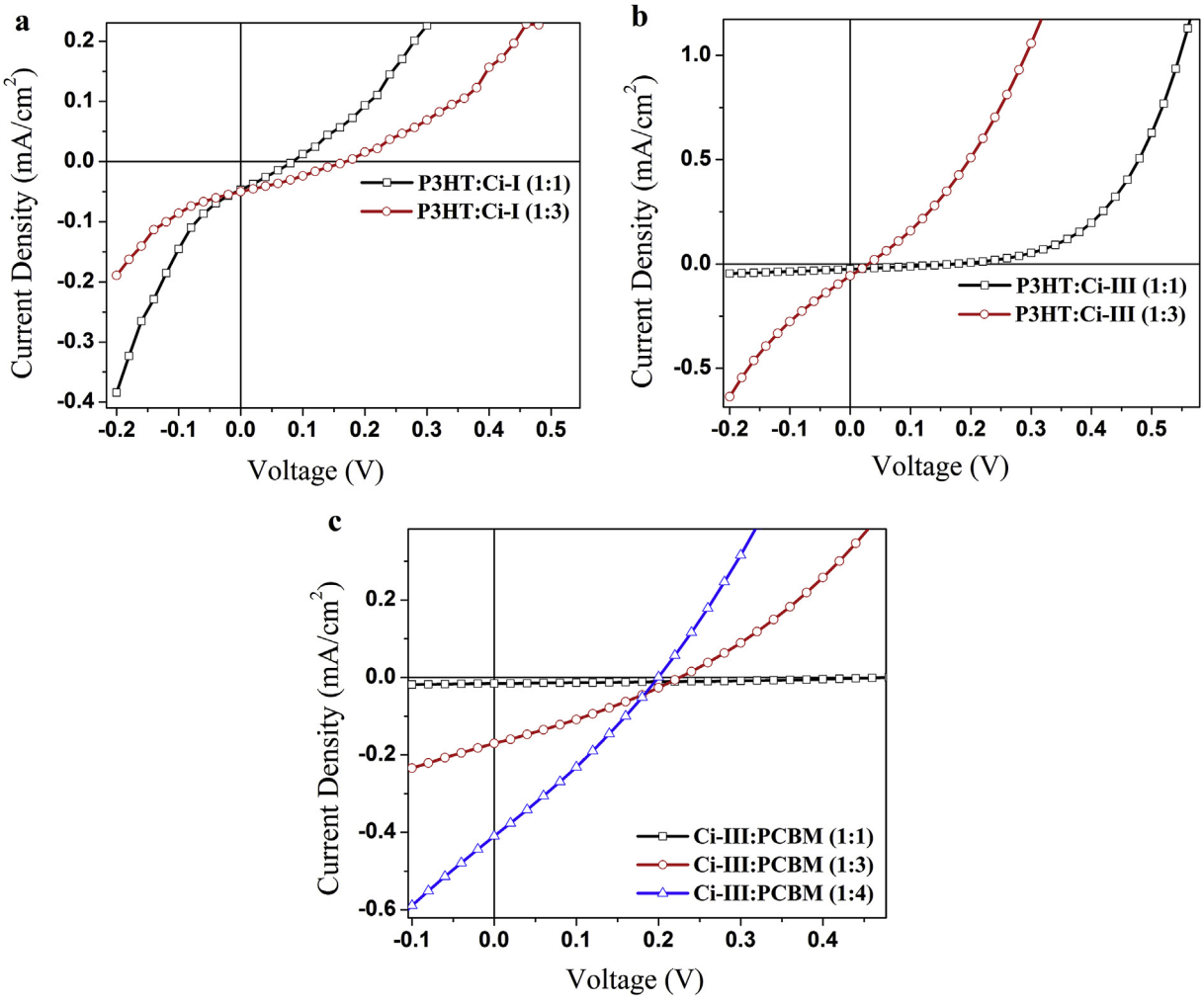

Fig. 8. J-V curves of photovoltaic devices using **(a)** P3HT:**Ci-I**, **(b)** P3HT:**Ci-III** and **(c) Ci-III**:PCBM blends with different mixing ratios as active layer.

Table 4
OPV parameters of normal BHJ devices prepared from cibalackrot dyes.

Active Layer		V_{oc} (mV)	I_{sc} (mA/cm^2)	FF	η
Binary Structure	w:w				
P3HT:**Ci-I**	1:1	220	0.005	0.50	0.003
P3HT:**Ci-I**	1:3	160	0.005	0.30	0.002
P3HT:**Ci-III**	1:1	180	0.020	0.26	0.001
P3HT:**Ci-III**	1:3	40	0.060	0.35	0.001
Ci-III:PCBM	1:1	560	0.010	0.35	0.002
Ci-III:PCBM	1:3	220	0.170	0.30	0.010
Ci-III:PCBM	1:4	200	0.410	0.28	0.020

UV–vis results in the range of 400–700 nm with a maximum of ~4.3% at 500 nm. Photovoltaic conversion efficiencies achieved with these used dyes were lower compared to relative analogues like indigo dyes, which is attributed to their much higher dielectric constant.

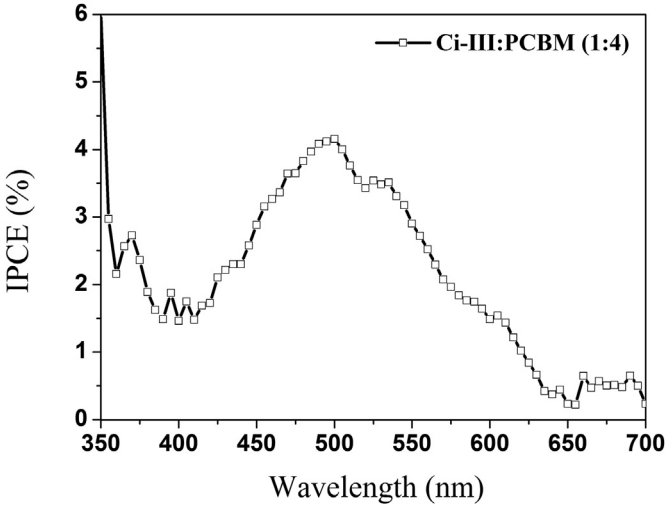

Fig. 9. IPCE graph for photovoltaic device using **Ci-III**:PCBM (1:4) blend as active layer.

4. Conclusions

We synthesized and investigated cibalackrot type donor or acceptor main cores with variations in the position of bromine group for charge transfer process. By changing the bromine position from the peripheral phenyl side to fused phenyl ring, the UV–vis absorbance gave a remarkable red shift in visible maximum of **Ci-III** dye because of the combination effect of both bromine auxochrome contribution and ICT possibility. **Ci-III** dye gave an increased current in conventional OPV device either as p-type or as

n-type semiconductor, while there is no current for **Ci-II** dye in this type of device. These findings demonstrated the potential use of small molecule cibalackrot dyes substituted with 3,10 positions of fused phenyl ring for promising photovoltaic devices.

Acknowledgements

This study was financed by the Scientific and Technological Research Council of Turkey with the project number of 113Z250. We also thank to Ege University for the support of the use of Gaussian 09 W program for theoretical DFT calculations.

Appendix A. Supplementary data

Supplementary data related to this article can be found at https://doi.org/10.1016/j.molstruc.2018.07.009.

References

[1] P.M. Beaujuge, C.M. Amb, J.R. Reynolds, Spectral engineering in π-conjugated polymers with intramolecular donor–acceptor interactions, Accounts Chem. Res. 43 (11) (2010) 1396–1407.
[2] H.-Y. Chen, J. Hou, S. Zhang, Y. Liang, G. Yang, Y. Yang, L. Yu, Y. Wu, G. Li, Polymer solar cells with enhanced open-circuit voltage and efficiency, Nat. Photon. 3 (11) (2009) 649–653.
[3] G. Engi, Über neue derivate des indigos und anderer indigoider farbstoffe, Angew. Chem. 27 (20) (1914) 144–148.
[4] H. Schmidt, Indigo – 100 jahre industrielle synthese, Chem. Unserer Zeit 31 (3) (1997) 121–128.
[5] E.D. Glowacki, G. Voss, N.S. Sariciftci, 25th Anniversary article: progress in chemistry and applications of functional indigos for organic electronics, Adv. Mater. 25 (47) (2013) 6783–6800.
[6] B. He, A.B. Pun, D. Zherebetskyy, Y. Liu, F. Liu, L.M. Klivansky, A.M. McGough, B.A. Zhang, K. Lo, T.P. Russell, L. Wang, Y. Liu, New form of an old natural dye: bay-annulated indigo (Bai) as an excellent electron accepting unit for high performance organic semiconductors, J. Am. Chem. Soc. 136 (42) (2014) 15093–15101.
[7] R. Shinar, E.D. Glowacki, I. Kymissis, L. Leonat, G. Voss, M. Bodea, Z. Bozkurt, M. Irimia-Vladu, S. Bauer, N.S. Sariciftci, Natural and nature-inspired semiconductors for organic electronics, Proc. SPIE 8118 (2011), 81180M(1–10).
[8] J. Seixas de Melo, R. Rondão, H.D. Burrows, M.J. Melo, S. Navaratnam, R. Edge, G. Voss, Photophysics of an indigo derivative (keto and leuco structures) with singular properties, J. Phys. Chem. A 110 (51) (2006) 13653–13661.
[9] B. He, D. Zherebetskyy, H. Wang, M.A. Kolaczkowski, L.M. Klivansky, T. Tan, L. Wang, Y. Liu, Rational tuning of high-energy visible light absorption for panchromatic small molecules by a two-dimensional conjugation approach, Chem. Sci. 7 (6) (2016) 3857–3861.
[10] M.A. Kolaczkowski, B. He, Y. Liu, Stepwise bay annulation of indigo for the synthesis of desymmetrized electron acceptors and donor-acceptor constructs, Org. Lett. 18 (2016) 5224–5227.
[11] K.J. Fallon, N. Wijeyasinghe, N. Yaacobi-Gross, R.S. Ashraf, D.M.E. Freeman, R.G. Palgrave, M. Al-Hashimi, T.J. Marks, I. McCulloch, T.D. Anthopoulos, H. Bronstein, A Nature-inspired conjugated polymer for high performance transistors and solar cells, Macromolecules 48 (15) (2015) 5148–5154.
[12] B. He, W.T. Neo, T.L. Chen, L.M. Klivansky, H. Wang, T. Tan, S.J. Teat, J. Xu, Y. Liu, Low bandgap conjugated polymers based on a nature-inspired bay-annulated indigo (Bai) acceptor as stable electrochromic materials, ACS Sustain. Chem. Eng. 4 (5) (2016) 2797–2805.
[13] J.R. Knutson, J.M. Beechem, L. Brand, Simultaneous analysis of multiple fluorescence decay curves - a global approach, Chem. Phys. Lett. 102 (6) (1983) 501–507.
[14] M. Zuker, A.G. Szabo, L. Bramall, D.T. Krajcarski, B. Selinger, Delta-function convolution method (DFCM) for fluorescence decay experiments, Rev. Sci. Instrum. 56 (1) (1985) 14–22.
[15] J. Pommerehne, H. Vestweber, W. Guss, R.F. Mahrt, H. Bassler, M. Porsch, J. Daub, Efficient 2-layer LEDs on a polymer blend basis, Adv. Mater. 7 (6) (1995) 551–554.
[16] M.J. Frisch, G.W. Trucks, H.B. Schlegel, G.E. Scuseria, M.A. Robb, J.R. Cheeseman, G. Scalmani, V. Barone, B. Mennucci, G.A. Petersson, H. Nakatsuji, M. Caricato, X. Li, H.P. Hratchian, A.F. Izmaylov, J. Bloino, G. Zheng, J.L. Sonnenberg, M. Hada, M. Ehara, K. Toyota, R. Fukuda, J. Hasegawa, M. Ishida, T. Nakajima, Y. Honda, O. Kitao, H. Nakai, T. Vreven, J.A. Montgomery Jr., J.E. Peralta, F. Ogliaro, M.J. Bearpark, J. Heyd, E.N. Brothers, K.N. Kudin, V.N. Staroverov, R. Kobayashi, J. Normand, K. Raghavachari, A.P. Rendell, J.C. Burant, S.S. Iyengar, J. Tomasi, M. Cossi, N. Rega, N.J. Millam, M. Klene, J.E. Knox, J.B. Cross, V. Bakken, C. Adamo, J. Jaramillo, R. Gomperts, R.E. Stratmann, O. Yazyev, A.J. Austin, R. Cammi, C. Pomelli, J.W. Ochterski, R.L. Martin, K. Morokuma, V.G. Zakrzewski, G.A. Voth, P. Salvador, J.J. Dannenberg, S. Dapprich, A.D. Daniels, Ö. Farkas, J.B. Foresman, J.V. Ortiz, J. Cioslowski, D.J. Fox, Gaussian 09, Gaussian, Inc., Wallingford, CT, USA, 2009.
[17] W. Kohn, L.J. Sham, Self-consistent equations including exchange and correlation effects, Phys. Rev. 140 (4A) (1965). A1133–A1138.
[18] C. Goh, R.J. Kline, M.D. McGehee, E.N. Kadnikova, J.M.J. Fréchet, Molecular-weight-dependent mobilities in regioregular poly(3-hexyl-thiophene) diodes, Appl. Phys. Lett. 86 (12) (2005), 122110(1–3).
[19] A. Carbone, B.K. Kotowska, D. Kotowski, Space-charge-limited current fluctuations in organic semiconductors, Phys. Rev. Lett. 95 (23) (2005), 236601(1–4).
[20] S. Icli, H. Icil, A thermal and photostable reference probe for Q_f measurements: chloroform soluble perylene 3,4,9,10-tetracarboxylic acid-bis-N,N'-dodecyl diimide, Spectrosc. Lett. 29 (7) (1996) 1253–1257.